Cycling speeds in crosswinds

C. Clanet [1,*] Hector Abel,[1] E. Brunet,[2] Francesco Grasso,[3] C. Robert,[4] and C. Cohen[1]

[1]*LadHyX, UMR7646 du CNRS, Ecole Polytechnique, 91128 Palaiseau, France*
[2]*FFC, 1 rue Laurent Fignon, 78180 Montigny-Le-Bretonneux, France*
[3]*DynFluid Laboratory, Cnam-Arts et Métiers, Paris 3, France*
[4]*Institut Aérotechnique (IAT-CNAM), 15, rue Marat, 78210 Saint-Cyr-l'École, France*

Using a large-scale wind tunnel equipped with an aerodynamic balance mounted on a rotating turntable, we first study the aerodynamic force exerted on a cyclist in time trial position from head to tailwind limits. A theoretical model for the aerodynamic force is developed to show the origin of the different experimental features. The theoretical analysis is then extended to the power dissipated in crosswinds and it is shown that the expression commonly used in the literature only holds in the pure head and tailwind limits but must be corrected in the general case of a crosswind. A new analytical expression for the total aerodynamic power is derived and used to determine the cycling speed in arbitrary crosswind conditions.

I. INTRODUCTION

Cycling started with the pedal-less running machine invented by Drais [1] who established on June 12, 1817, at the age of 33, the first unofficial hour record of the order of 14 km [2,3].

The first official hour record was established by Henri Desgrange in 1893 (35.325 km) at the Buffalo velodrome in Paris [4], and pushed by Victor Campenaerts up to 55.089 km in April 2019 at the Aguascalientes cycling track [3]. As shown in books [5] and reviews [3,6], this increase in velocity is mainly due to the reduction of the aerodynamic resistance.

This resistance changes in road races due to wind, which has long been recognized as a major factor in cycling performances [7,8]. Crosswinds in particular are considered as a crucial factor for cyclist safety [9–11] and produce echelon-type patterns in pelotons [12,13]. Due to atmospheric boundary layers and nonuniform topography, real wind conditions are difficult to analyze [14] and wind-tunnel experiments are needed. As for sailing, the discussion of the effect of wind on a cyclist implies the definition of the true wind and of the apparent wind [15].

This definition is presented in Fig. 1: in the reference frame of the road [Fig. 1(a)], the direction of the true wind of velocity $\underline{U}_w$ and that of the cyclist of velocity $\underline{U}_c$ differ by the angle α (wind angle). In the reference frame of the bike [Fig. 1(b)] the apparent wind of velocity $\underline{U} = \underline{U}_w - \underline{U}_c$ makes the angle β (yaw angle) with the direction of motion. The main difference with sailing is that the cyclist moves even with zero true wind. In that limit, the apparent wind reduces to $\underline{U} = -\underline{U}_c$ which is a pure headwind. A consequence of this remark is that even if all true wind directions have the same probability, the motion of the cyclist induces a statistical bias that tends to favor apparent headwinds [16,17].

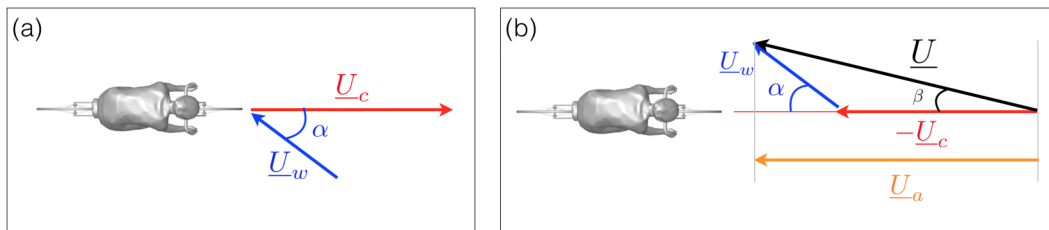
*clanet@ladhyx.polytechnique.fr

FIG. 1. Sketch of the cyclist in a crosswind: (a) The cyclist velocity $\underline{U}_c$ and the wind velocity $\underline{U}_w$ make an angle α (wind angle): $\alpha = 0°$ is headwind and $\alpha = 180°$ is tailwind. (b) In the reference frame of the bike, the apparent wind $\underline{U} = \underline{U}_w - \underline{U}_c$ makes an angle β (yaw angle) with the direction of motion. This apparent wind has the intensity $U_a = U_c + U_w \cos \alpha$ in the cycling direction. The cyclist is taken from Malizia and Blocken [3] (courtesy of Bert Blocken, Eindhoven University of Technology and KU Leuven).

By using a full-scale bicycle with a mannequin, Fintelman *et al.* [10] have studied experimentally the effect of crosswind for yaw angles in the range $\beta = 0°$ to $\beta = 90°$. These authors show that the drag is maximum at $\beta = 0°$ and decreases down to almost zero at $\beta = 90°$, whereas the side force exhibits opposite trends, being null at $\beta = 0°$ and maximum at $\beta = 90°$. Similar behaviors are reported by Kraemer *et al.* using model rigid cyclists at the scale 1/32 [13].

The associate question of the total aerodynamic power dissipated by a cyclist moving at velocity $\underline{U}_c$ in a wind of velocity $\underline{U}_w$ [Fig. 1(a)], was first considered in 1894 by Bourlet [18] and more recently by Martin *et al.* [8]. In the reference frame of the cyclist [Fig. 1(b)], the apparent wind $\underline{U}$ has a component $U_a = U_c + U_w \cos \alpha$ in the direction of motion and the expression for the total aerodynamic power was proposed to be

$$P_{AC} = \tfrac{1}{2} \rho S C_{D0} U_a^2 \, U_c, \tag{1}$$

where ρ is the air density, and SC_{D0} is the frontal drag area based on the frontal area at zero yaw angle S and the corresponding drag coefficient C_{D0} [3].

In the present paper we carry out a full-scale experiment with a cyclist in time trial position exploring the entire wind spectrum from pure head to pure tail limits. The experimental setup used to quantify the effect of the intensity and direction of the wind is presented in Sec. II. We thus obtain a complete set of measurements which are presented in Sec. III and then used to establish a theoretical model for the aerodynamic force discussed in Sec. IV. The theoretical study is then used in Sec. V to establish the expression of the total aerodynamic power for any crosswind. This expression is finally used in Sec. VI to calculate the cycling speed for any wind intensity and direction.

II. EXPERIMENTAL SETUP

The general setup is presented in Fig. 2: a cyclist in time trial position is fixed on a rotating turntable in the S4 wind tunnel of the Institut Aerotechnique (IAT) whose characteristics are described in Sec. II C. The wind direction in the vein defines the $\underline{e}_x$ axis which is the apparent wind direction ($\underline{U} = U\underline{e}_x$). The yaw angle β is controlled by the turntable. For $\beta = 0$ the cyclist experiences a pure headwind force while for $\beta = 180°$ he feels a back force. This setup thus allows to tune precisely the apparent wind intensity and direction independently.

Concerning the forces, the cyclist experiences the total aerodynamic force $\underline{F}_A = \underline{F}_D + \underline{F}_L + \underline{F}_S$ which is composed of the drag force $\underline{F}_D$, of the lift force $\underline{F}_L$ and of the side force $\underline{F}_S$. Since the lift force on a cyclist is small [19], the total aerodynamic force reduces to $\underline{F}_A = \underline{F}_D + \underline{F}_S$.

The orientation of the cyclist with respect to the flow is varied between $\beta = 0°$ [Fig. 3(a)] and $\beta = 180°$ [Fig. 3(c)] with angle increments of $\Delta\beta = 20°$. The perpendicular direction $\beta = 90°$ [Fig. 3(b)] is added to this set (0,20,40,60,80,90,100,120,140,160,180). For each angle, the drag
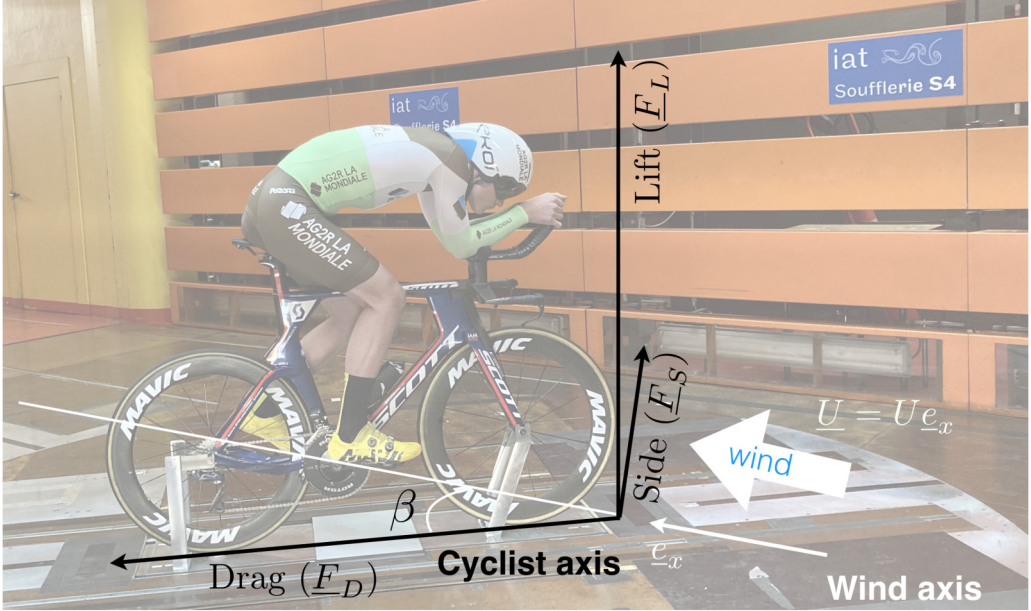
FIG. 2. Setup and conventions used to study the wind force on a cyclist.

force $\underline{F}_D$ and the side force $\underline{F}_S$ are measured by the balance, from which the forces $\underline{F}_x$ and $\underline{F}_y$, respectively in the x and y directions are deduced [Fig. 3(d)]:

$$\underline{F}_x = (F_D \cos\beta + F_S \sin\beta)\underline{e}_x \quad \text{and} \quad \underline{F}_y = (-F_D \sin\beta + F_S \cos\beta)\underline{e}_y, \tag{2}$$

where $\underline{e}_x$ and $\underline{e}_y$ are the unit vectors in the x and y directions. The resultant aerodynamic force acting on the cyclist is shown in Fig. 3(d): $\underline{F}_A = \underline{F}_D + \underline{F}_S = \underline{F}_x + \underline{F}_y$.

In the following, the different intensities of forces will be expressed as

$$F_\lambda = \tfrac{1}{2}\rho SC_\lambda U^2, \tag{3}$$

where SC_λ is the area coefficient associated to the component λ ($D = $ drag, $S = $ side, $x = x$ direction, $y = y$ direction).

A. The cyclist and his equipment

The experiments have been conducted with a time trial specialist from the AG2R Citroën U23 Team (21 years old, 1.85 m, 77 kg). To reproduce the real conditions during the experiments, the cyclist has used his own equipment: bike (Scott Plasma 5, Switzerland), skin suit (Rosti, France), helmet with visor (Ekoi TTRB, France), and cotton socks. Bike tubulars are 2-(Vittoria Corsa, Italia) inflated at a pressure of 8 bars.

B. Three different wheel sets

To evaluate the influence of the wheels, we have used the three wheel sets presented in Fig. 4: Set 1 = spokes wheels (Mavic CXR 80, France) with 24 spokes in the back and 16 spokes in the front; Set 2 = back disk wheel (Corima Paracular, France) and front 3 spokes wheel (Corima 3 spokes,
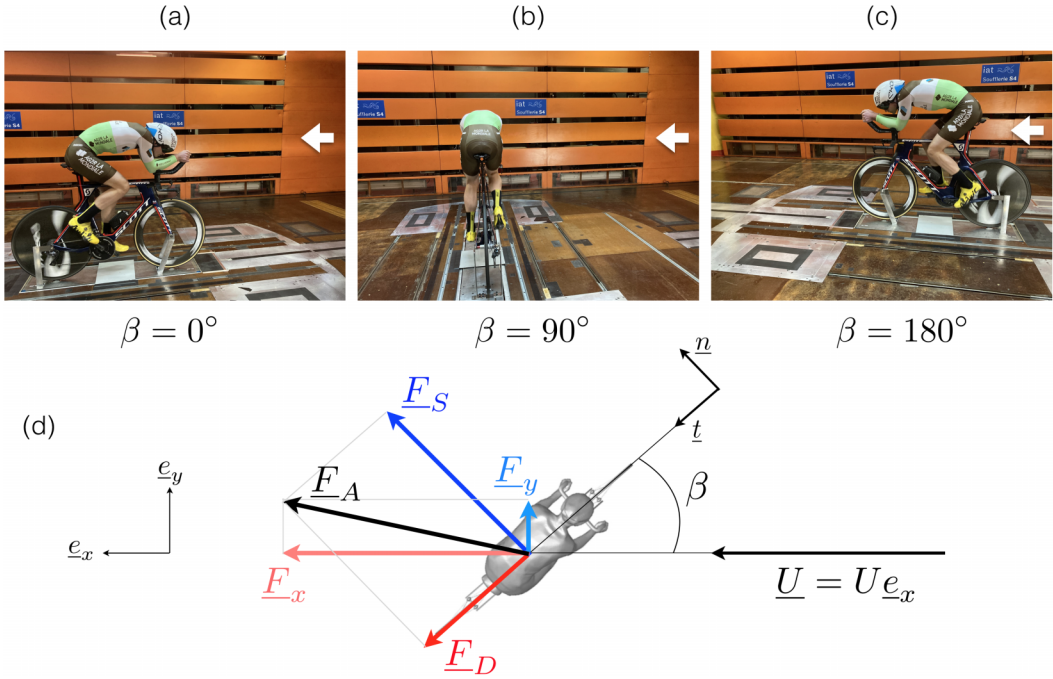
(a) $\beta = 0°$ (b) $\beta = 90°$ (c) $\beta = 180°$

(d)

FIG. 3. Experimental setup used to measure the wind force $\underline{F}_A$ on a cyclist: (a) pure headwind position ($\beta = 0°$), (b) perpendicular wind ($\beta = 90°$), (c) pure tailwind position ($\beta = 180°$), (d) conventions used to describe the forces acting on the cyclist. In panels (a–c), the white arrow indicates the direction of the flow.

France); Set 3 = back disk wheel (Corima Paracular, France) and front 16 spokes wheel (Mavic CXR 80, France).

C. Wind tunnel

Tests are carried out in the S4 wind tunnel of the Institut Aérotechnique at Saint-Cyr-l'Ecole. The facility is a subsonic wind tunnel (maximum speed 40 m/s, turbulence intensity 1%), with dimensions 5 m wide, 3 m high, and 10 m long. The wind tunnel is equipped with a 4 m diameter rotating turntable that incorporates a six-components aerodynamic balance and a dynamometer roller that allows to turn the wheels of the bicycle. A schematic of the wind tunnel and the main characteristics of the aerodynamic balance are given in the Appendix. Three wind speeds are
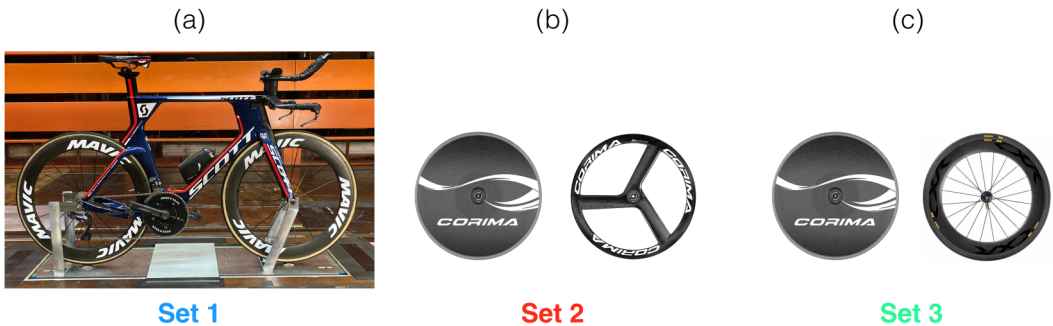

(a) Set 1   (b) Set 2   (c) Set 3

FIG. 4. Presentation of the three sets of wheels tested: (a) Set 1, (b) Set 2, (c) Set 3.
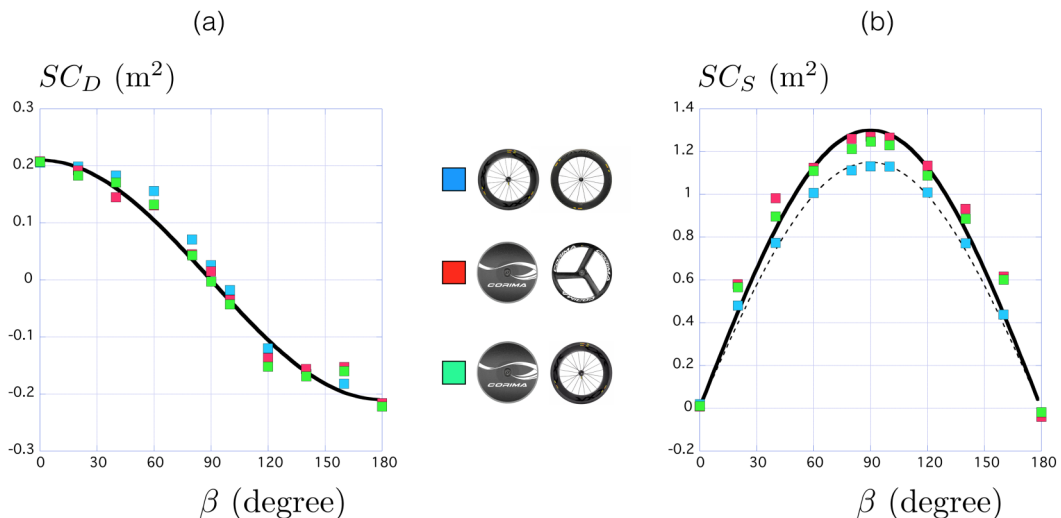
FIG. 5. Variation of the drag area SC_D (a) and of the side area SC_S (b) as a function of the direction of the apparent wind β using $U = 13.9\,\text{m/s}$ (50 km/h). The results obtained with wheel Set 1 are presented with blue squares. Red squares represent the results obtained with wheel Set 2 and green squares those of wheel Set 3. The solid line in panel (a) stands for the heuristic relation $SC_D = 0.21 \cos\beta$. The solid line in panel (b) stands for the heuristic relation $SC_S = 1.3 \sin\beta$ and the dashed line for $SC_S = 1.15 \sin\beta$.

considered $U_1 = 13.9$ m/s (50 km/h), $U_2 = 11.1$ m/s (40 km/h), and $U_3 = 16.7$ m/s (60 km/h). For each wind speed U_i the rotation of the wheels ω_i is adjusted so that $R\omega_i = U_i$, where $R = 339$ mm is the radius of the wheel. During the tests, the cyclist is asked to turn his legs at his natural spin rate. All the experiments are conducted at a pressure $p_{\text{atm}} = 100791$ Pa, temperature $T_{\text{atm}} = 293$ K corresponding to air density $\rho = 1.199$ kg/m^3.

III. EXPERIMENTAL RESULTS

A. Influence of the set of wheels

In this section, we discuss the influence of the wheels on the force acting on the cyclist, keeping constant the wind speed at $U = 13.9$ m/s (50 km/h) and varying the direction of the apparent wind β. Figure 5 reports the evolutions of the drag area SC_D (a) and of the side area SC_S (b) as a function of β. The three different sets of wheels are represented with three different colors (wheel Set 1 in blue, wheel Set 2 in red, and wheel Set 3 in green). We observe that the evolution of the drag area is similar for the three sets and can be approximated by the heuristic relation $SC_D = SC_{D0} \cos\beta$ with $SC_{D0} = 0.21$ m^2 (within 10% accuracy over the whole range of yaw angles β). The behavior of the side area SC_S is also similar for the three sets. Sets 2 and 3 having the same back wheels and different front ones are well fitted (within 5% accuracy over the whole range of β) by $SC_S = SC_{S90} \sin\beta$ with $SC_{S90} = 1.3$ m^2 whereas Set 1 is well described by $SC_{S90} = 1.15$ m^2 (within 3% accuracy over the whole range of β).

From the relations Eqs. (2) and (3) we deduce the x area SC_x [Fig. 6(a)] and the y area SC_y [Fig. 6(b)] on the cyclist. As expected, the x area is minimal for pure headwind and pure tailwind and exhibits a maximum for $\beta = 90°$.

Using the heuristic relations for SC_D and SC_S in Eq. (2) one deduces the following relations for the x area [solid line in Fig. 6(a)] and for the y area [solid line in Fig. 6(b)] on the cyclist:

$$SC_x = SC_{D0} + (SC_{S90} - SC_{D0}) \sin^2\beta \quad \text{and} \quad SC_y = (SC_{S90} - SC_{D0}) \sin 2\beta / 2. \tag{4}$$
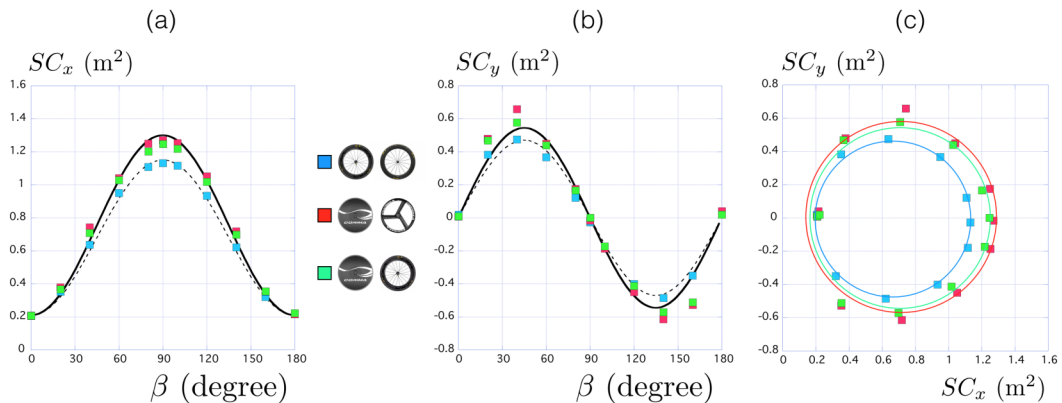
FIG. 6. Variation of the x area SC_x (a) and of the y area SC_y (b) as a function of the apparent wind direction β using $U = 13.9$ m/s (50 km/h). The resulting polar curve $SC_y(SC_x)$ is presented in panel (c). Wheel Set 1, blue; wheel Set 2, red; wheel Set 3, green.

These equations show that both x and y drag areas are minimum for pure headwinds ($\beta = 0°$) and pure back winds ($\beta = 180°$). F_x reaches a maximum at $\beta = 90°$ (namely, when the apparent wind is perpendicular to the cyclist direction), whereas the cyclist experiences maximum force in the y direction when the apparent wind direction is at $\beta = 45°$ and $\beta = 135°$.

From the x and y forces, we construct the polar curve of a cyclist $SC_y(SC_x)$ presented in Fig. 6(c). Apart from its quasicircular shape we observe a clear separation of the three sets of wheels: Set 2 (red) has a larger surface than Set 3 (green) which has itself a larger surface than Set 1 (blue).

The above experimental results provide an heuristic expression for the total aerodynamic force $\underline{F}_A$ acting on a cyclist in crosswind (Fig. 3):

$$\underline{F}_A = \frac{1}{2}\rho U^2 \begin{bmatrix} SC_{D0}\cos\beta \ \underline{t} \\ SC_{S90}\sin\beta \ \underline{n} \end{bmatrix} = \frac{1}{2}\rho U^2 \begin{bmatrix} [SC_{D0} + (SC_{S90} - SC_{D0})\sin^2\beta] \ \underline{e}_x \\ 1/2(SC_{S90} - SC_{D0})\sin 2\beta \ \underline{e}_y \end{bmatrix}. \tag{5}$$

B. Influence of the velocity

The influence of the apparent wind velocity on the drag and side areas has been measured using the bicycle equipped with paracular back and front wheels Corima 3B (wheel Set 2). Three different velocities have been considered $U = 11.1$ m/s (40 km/h), $U = 13.9$ m/s (50 km/h) and $U = 16.7$ m/s (60 km/h). The results reported in Fig. 7 show that both the drag area and the side area are unaffected by the wind velocity at any given yaw angle: over the whole range of yaw angles β, the difference observed between 16.7 m/s (orange squares) and 11.1 m/s (black squares) is less than 5%.

IV. SIMPLE MODEL FOR THE AERODYNAMIC FORCE ON A CYCLIST

The basic idea to model the flow around a cyclist consists in observing that the bicycle defines a plane perpendicular to the ground containing the two wheels and the frame and that the cyclist is a bluff body. As shown in Fig. 8(a) we thus decompose the flow around the cyclist in two distinct parts: the flow around a plate of incident angle β accounting for the bike (1) and the flow around a cylinder accounting for the cyclist (2). Following Hoerner [20], the flow around a plate induces an aerodynamic force perpendicular to the plate of the form $\underline{F}_{A1} = 1/2\rho SC_{D1}U^2 \sin\beta \ \underline{n}$. On the other side, the flow around a cylinder induces the aerodynamic force $\underline{F}_{A2} = 1/2\rho SC_{D2}U^2 \ \underline{e}_x$. Using the decomposition $\underline{F}_A = \underline{F}_{A1} + \underline{F}_{A2}$ together with the geometrical relations $\underline{e}_x = \cos\beta \ \underline{t} + \sin\beta \ \underline{n}$ and
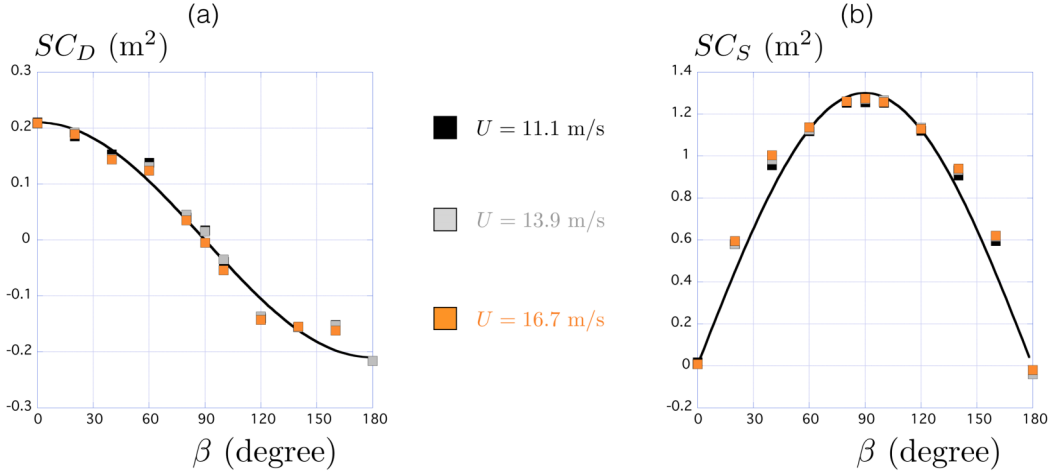
FIG. 7. Variation of the drag area SC_D (a) and of the side area SC_S (b) as a function of the direction of the apparent wind β at three different wind speeds: $U = 11.1$ m/s in black full squares, $U = 13.9$ m/s in gray full square and $U = 16.7$ m/s in orange full square and using wheel set 2. The solid line in (a) represents the heuristic relation $SC_D = 0.21 \cos \beta$. The solid line in panel (b) indicates the heuristic relation $SC_S = 1.3 \sin \beta$.

$\underline{e}_y = -\sin \beta \, \underline{t} + \cos \beta \, \underline{n}$ we get

$$\underline{F}_A = \frac{1}{2}\rho U^2 \begin{bmatrix} SC_{D2} \cos \beta \, \underline{t} \\ (SC_{D1} + SC_{D2}) \sin \beta \, \underline{n} \end{bmatrix} = \frac{1}{2}\rho U^2 \begin{bmatrix} \left[SC_{D2} + SC_{D1} \sin^2 \beta \right] \underline{e}_x \\ SC_{D1}/2 \sin 2\beta \, \underline{e}_y \end{bmatrix}. \tag{6}$$

This aerodynamic force is identical to the one obtained experimentally provided the identification $SC_{D1} = SC_{S90} - SC_{D0}$ and $SC_{D2} = SC_{D0}$. While looking for the corresponding polar curve, we deduce the following relationship between the y and x components:

$$\left[\frac{SC_x}{SC_{D1}/2} - \left(\frac{SC_{D2}}{SC_{D1}/2} + 1 \right) \right]^2 + \left(\frac{SC_y}{SC_{D1}/2} \right)^2 = 1. \tag{7}$$

This equation describes a circle of radius $R = SC_{D1}/2$ the center of which is located on the horizontal axis at a distance $R + SC_{D2}$ from the origin. This circle is presented in Fig. 8(b) and allows us to understand the features obtained experimentally [Fig. 6(c)].

V. AERODYNAMIC POWER

The power P_A dissipated by the aerodynamic force writes $P_A = \underline{F}_A . \underline{U}_c$. Since $\underline{F}_A = \underline{F}_D + \underline{F}_S = F_D \, \underline{t} + F_S \, \underline{n}$ and $\underline{U}_c = -U_c \, \underline{t}$ one deduces: $P_A = -F_D U_c$. Using the expression of the drag force
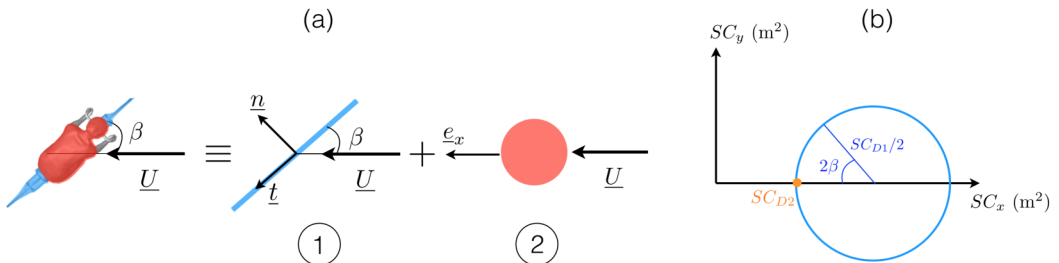

FIG. 8. (a) Decomposition of the flow around the cyclist. (b) Polar curve associated with Eq. (7).

$F_D = 1/2\rho SC_D(\beta)U^2$, the aerodynamic power takes the form

$$P_A = -\frac{1}{2}\rho SC_D(\beta)\left(U_c^2 + U_w^2 + 2U_cU_w\cos\alpha\right)U_c, \tag{8}$$

where the square of the apparent wind is deduced from the composition presented in Fig. 1(b) as $U^2 = (U_c + U_w\cos\alpha)^2 + (U_w\sin\alpha)^2$. If P_A is negative, then power is dissipated by aerodynamic resistance. When $SC_D(\beta) < 0$ the sign changes and the aerodynamic force becomes propulsive. Using the heuristic relation $SC_D = SC_{D0}\cos\beta$ $[SC_{D0} = SC_D(\beta = 0)]$ one deduces that the resistance-propulsion transition occurs for $\beta = 90°$. Since $\cos\beta = (U_c + U_w\cos\alpha)/U$, Eq. (8) can be rewritten as

$$P_A = -\frac{1}{2}\rho SC_{D0}\sqrt{(U_c + U_w\cos\alpha)^2 + (U_w\sin\alpha)^2}\,(U_c + U_w\cos\alpha)\,U_c. \tag{9}$$

This expression reduces (in absolute value) to the classical expression $P_{AC} = 1/2\rho SC_{D0}U_a^2U_c$ [Eq. (1)] only for $\sin\alpha = 0$, namely, in either pure headwind ($\alpha = 0°$) or pure tailwind ($\alpha = 180°$). Apart from these two limits the aerodynamic power predicted by Eq. (9) is larger than the one expected by the classical expression. The perpendicular wind case $\alpha = 90°$ allows to illustrate the difference between both expressions: in this limit, the classical expression predicts that the aerodynamic power is independent of the wind speed $P_{AC}(\alpha = 90°) = 1/2\rho SC_{D0}U_c^3$. On the contrary, Eq. (9) predicts that the aerodynamic power does depend on the wind speed: $|P_A| = 1/2\rho SC_{D0}\sqrt{U_c^2 + U_w^2}\,U_c^2$; the larger the wind speed the larger the dissipation.

VI. WIND IMPACT ON CYCLIST SPEED

The discussion is initially conducted assuming a straight and horizontal road with a constant cyclist velocity. To analyze the impact of the aerodynamic resistance on the cyclist speed we first introduce the zero true wind limit (Sec. VI A). The impact of wind on this velocity is then determined through a balance between the power delivered by the cyclist and the new expression of the aerodynamic power dissipation (Sec. VI B). The role of rolling resistance and road slope are discussed in Secs. VI C and VI D, respectively.

A. The zero true wind limit

When $U_w = 0$, Eq. (9) simply writes $|P_{A0}| = 1/2\rho SC_{D0}U_{c0}^3$ where $U_{c0} = U_c(U_w = 0)$ and $P_{A0} = P_A(U_w = 0)$. In the limit where the aerodynamic resistance dominates (rolling and slope contributions are discussed in a second step) the steady velocity of the cyclist is achieved by balancing this aerodynamic resistance with the power, P_m, delivered by the muscle [7,21]. This balance, $P_m = |P_{A0}|$, leads to the expression of the zero wind steady velocity:

$$U_{c0} = \left(\frac{2P_m}{\rho SC_{D0}}\right)^{1/3}. \tag{10}$$

With $P_m = 200$ W and $SC_{D0} = 0.25$ m^2 one finds $U_{c0} = 11$ m/s. This velocity increases up to 13.9 m/s (50 km/h) for $P_m = 400$ W, which is the typical velocity observed in professional flat time trial [21].

B. Cyclist velocity in a crosswind

Assuming that the muscle power P_m is not affected by the wind ($P_m = |P_{A0}|$), we use the balance $|P_A| = P_m$ to obtain, via Eq. (9), the equation of the cyclist velocity in a crosswind:

$$\sqrt{(\bar{U}_c + \bar{U}_w\cos\alpha)^2 + (\bar{U}_w\sin\alpha)^2}(\bar{U}_c + \bar{U}_w\cos\alpha)\bar{U}_c = 1, \tag{11}$$

where $\bar{U}_c = U_c/U_{c0}$ and $\bar{U}_w = U_w/U_{c0}$. This nonlinear equation is solved numerically and the results are shown in Fig. 9(a). The isovalues of the reduced velocity U_c/U_{c0} are represented in the wind
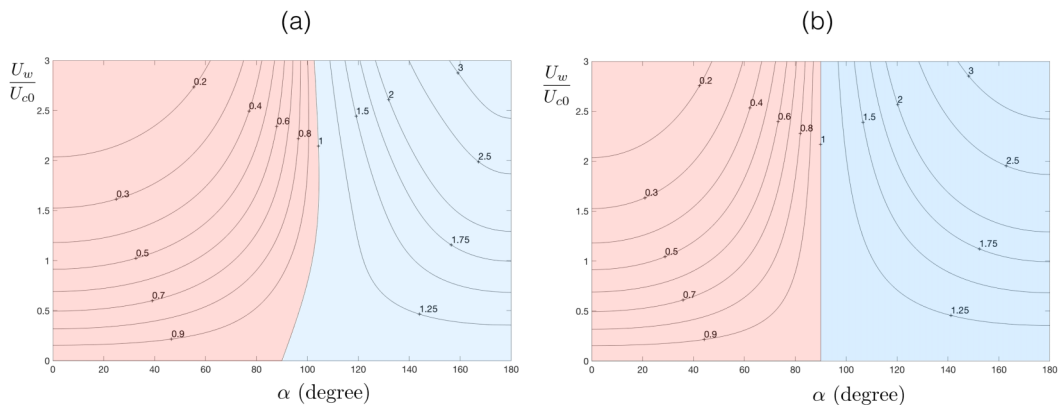
FIG. 9. Isovelocity lines U_c/U_{c0} in the wind phase space $(\alpha, U_w/U_{c0})$. The red region corresponds to the headwind domain whereas the blue region to the tailwind. Panel (a) represents the solution obtained from Eq. (11); panel (b) reports the predicted isovelocity lines obtained from the classical Eq. (1) reformulated as in Eq. (12).

phase space $(\alpha, U_w/U_{c0})$. The red region corresponds to the domain where the cyclist velocity in the wind is smaller than his velocity without wind ($U_c/U_{c0} < 1$). This "headwind-type" domain extends from $\alpha = 0$ to a value larger than $90°$ which depends on the intensity of the wind. The blue region corresponds to the domain where the velocity in the wind is larger than the one achieved in the zero wind limit ($U_c/U_{c0} > 1$) which is the "tailwind-type" domain. At the interface between these two zones, one finds the isovalue $\bar{U}_c = 1$ where the wind does not affect the velocity of the cyclist. The isovelocity curves exhibit a hyperbolic behavior: at low relative wind velocities ($U_w/U_{c0} < 1$), they are almost horizontal which means that the cyclist velocity is nearly independent of the wind direction. However, it changes with the wind intensity. On the contrary, at large relative wind velocities ($U_w/U_{c0} > 1$), the isovelocity lines are almost vertical which means that the cyclist speed becomes very sensitive to the wind direction.

This predicted velocity of the cyclist in the wind is compared with the one obtained from the classical Eq. (1), which is recast for comparison as

$$\sqrt{(\bar{U}_c + \bar{U}_w \cos\alpha)^2}(\bar{U}_c + \bar{U}_w \cos\alpha)\bar{U}_c = 1. \tag{12}$$

The results are presented in Fig. 9(b). The figure shows that the formula that we obtained to estimate the cyclist velocity using the new expression for the aerodynamic power [Eq. (9)], and the one obtained by applying the classical expression yield the same results in the limits of pure headwind ($\alpha = 0°$) and pure tailwind ($\alpha = 180°$). For a side wind perpendicular to the road (namely, for $\alpha = 90°$) the latter yields $U_c/U_{c0} = 1$ independently of the wind intensity, whereas the new relation correctly predicts that the cyclist velocity decreases by an amount that depends on the wind intensity.

C. Cyclist velocity in a crosswind with rolling friction

According to Martin *et al.* [8], the power dissipated by rolling resistance $P_{RR} = C_{RR}MgU_c$ is the second most important dissipation after the aerodynamic resistance. The balance $|P_A| + P_{RR} = P_m$ leads to the equation for the cyclist velocity:

$$\sqrt{(\bar{U}_c + \bar{U}_w \cos\alpha)^2 + (\bar{U}_w \sin\alpha)^2}(\bar{U}_c + \bar{U}_w \cos\alpha)\bar{U}_c + \epsilon_{RR}\bar{U}_c = 1, \tag{13}$$

where $\epsilon_{RR} = 2C_{RR}Mg/(\rho SC_{D0}U_{c0}^2)$. Using typical values $C_{RR} = 0.004$, $M = 80$ kg, $SC_{D0} = 0.25$ m^2, and $P_m = 200$ W, one finds $U_{c0} = 11$ m/s and $\epsilon_{RR} = 0.17$.
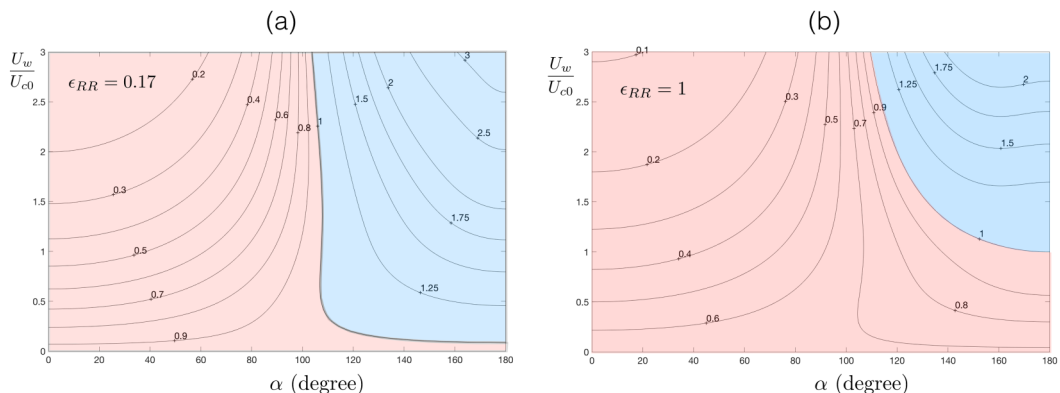
FIG. 10. Isovelocity lines U_c/U_{c0} in the wind phase space $(\alpha, U_w/U_{c0})$ for two different rolling friction: panel (a) $\epsilon_{RR} = 0.17$, panel (b) $\epsilon_{RR} = 1$.

The solution of Eq. (13) for $\epsilon_{RR} = 0.17$ is presented in Fig. 10(a). The first observation is that the red region spreads out through the full angle range in the limit of zero wind. This means that even without wind the cyclist will not reach the maximum speed U_{c0} due to the rolling friction. The blue region defined by $\bar{U}_c \geqslant 1$ is reduced but the general trend remains unchanged. Increasing the rolling friction to $\epsilon_{RR} = 1$ leads to the solution presented in Fig. 10(b). The blue region shrinks in the top right corner.

To further analyze the influence of the rolling resistance, we introduce the steady cyclist velocity in the zero wind limit, U_{c1}, that satisfies the following relation:

$$\tfrac{1}{2}\rho S C_{D0} U_{c1}^3 + C_{RR} M g U_{c1} = P_m = \tfrac{1}{2}\rho S C_{D0} U_{c0}^3. \tag{14}$$

This equation can be cast in a Tartaglia-type cubic equation:

$$\bar{U}_{c1}^3 + \epsilon_{RR}\bar{U}_{c1} = 1, \tag{15}$$

where $\bar{U}_{c1} = U_{c1}/U_{c0}$. The solution of Eq. (15) is

$$\bar{U}_{c1} = X - (\epsilon_{RR}/3)/X \quad \text{with} \quad X = \left(\frac{1 + \sqrt{1 + 4(\epsilon_{RR}/3)^3}}{2}\right)^{1/3}. \tag{16}$$

For $\epsilon_{RR} = 0.17$, one finds $\bar{U}_{c1} = 0.94$, and for $\epsilon_{RR} = 1$, one finds $\bar{U}_{c1} = 0.68$. If we now normalize the cyclist velocity by the zero-wind limit velocity U_{c1} obtained from the Tartaglia solution, then we observe in Fig. 11 that U_c/U_{c1} exhibits the same features observed for U_c/U_{c0} when plotted in the wind phase space $(\alpha, U_w/U_{c1})$. In this representation, the headwind (red region) and tailwind (blue region) domains become similar to the one obtained without friction and presented in Fig. 9(a).

D. Cyclist velocity in the wind with rolling friction and inclined road

The impact of a crosswind on the velocity of a cyclist climbing a slope G_r can easily be treated since the power associated to the slope writes $P_{PE} = G_r M g U_c$ [8,21]. This structure is identical to the one associated to the rolling friction, the road slope playing the same role as the rolling coefficient C_{RR}. The impact of a crosswind on the velocity of a cyclist climbing an inclined road can thus be treated using the analysis presented in Sec. VI C replacing C_{RR} by $C_{RR} + G_r$.

VII. CONCLUSION

The aerodynamic force exerted on a cyclist in a time trial position by an apparent crosswind of intensity U and yaw angle β is first studied experimentally in a large-scale wind tunnel. For the first
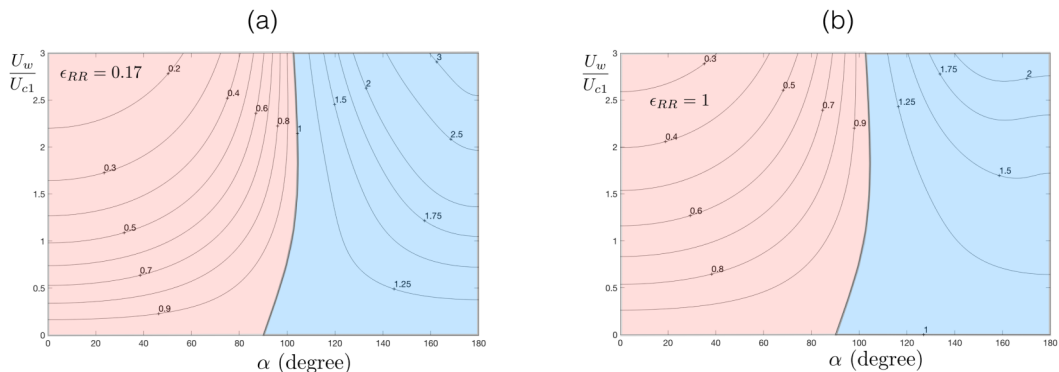
FIG. 11. Isovelocity lines U_c/U_{c1} in the wind phase space $(\alpha, U_w/U_{c1})$ for two different rolling friction: panel (a) $\epsilon_{RR} = 0.17$, panel (b) $\epsilon_{RR} = 1$.

time, the entire wind range direction from $\beta = 0°$ (pure headwind) to $\beta = 180°$ (pure tailwind) is explored, thus enabling the establishment of analytical relations for the drag and side areas:

$$SC_D = SC_{D0} \cos \beta \quad \text{and} \quad SC_S = SC_{S90} \sin \beta,$$

where SC_{D0} and SC_{S90} are constants that have been found to be of the order of $0.21\,\text{m}^2$ and $1.3\,\text{m}^2$, respectively.

A theoretical model based on the decomposition of the flow around the cyclist as the sum of the flow around a flat plate (accounting for the plane defined by the bike) and the one around a cylinder (accounting for the bluff body of the cyclist) is then developed. The model is shown to be able to account for the main aerodynamic features observed experimentally.

These quantitative results obtained for the force exerted by the wind on a cyclist are then used to establish the expression of the total aerodynamic power associated to an arbitrary crosswind. Considering a cyclist of velocity U_c cycling in a wind of intensity U_w and direction α ($\alpha = 0$ being headwind), the expression of the total aerodynamic power dissipated in crosswinds is found to be

$$P_A = -\tfrac{1}{2}\rho SC_{D0} \sqrt{(U_c + U_w \cos \alpha)^2 + (U_w \sin \alpha)^2}\,(U_c + U_w \cos \alpha)\,U_c.$$

Using this new expression for the total aerodynamic power we finally study the impact of the wind on the steady velocity of the cyclist and determine the velocity change compared to the zero wind limit as a function of the relative wind speed and direction.

The impact of rolling resistance and road slope are finally considered and a general framework is presented to address the impact of any crosswind on a cyclist.
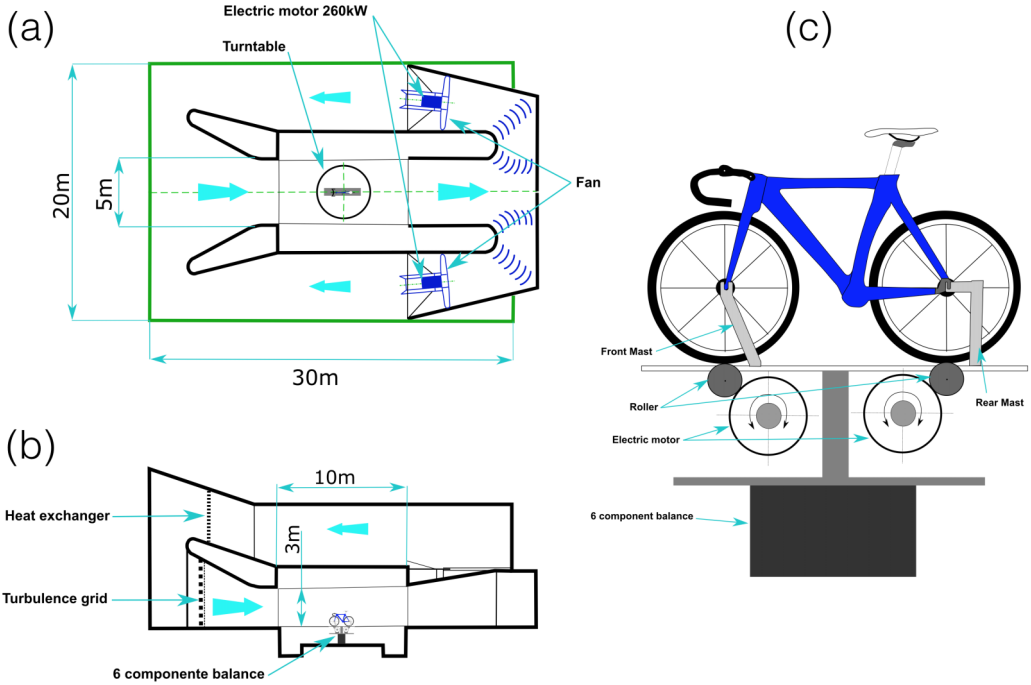
FIG. 12. (a) Top view scheme of S4 wind tunnel. (b) Side view scheme of S4 wind tunnel. (c) Detail of the bike connection to the aerodynamic balance.

APPENDIX: MAIN CHARACTERISTICS OF THE S4 WIND TUNNEL OF IAT

A schematic of the S4 wind tunnel is shown in Fig. 12 and we detail below the measurement of the incoming velocity U, the size of the boundary layer, the accuracy of the balance and the cyclist setup.

1. Wind speed measurement

The dynamic pressure $P_{\mathrm{dyn}} = P_{\mathrm{tot}} - P_{\mathrm{stat}}$ is measured from a total pressure probe (P_{tot}) installed at the inlet of the test section and from two static pressure taps (P_{stat}) symmetrically positioned on the lateral walls at the center of the test section using a differential pressure transducer. The atmospheric pressure is measured by a barometric gage, the air temperature is measured in the test section by means of a thermocouple and the air density is calculated applying the equation of state. The wind velocity is then obtained from the dynamic pressure definition:

$$U = \sqrt{\frac{2P_{\mathrm{dyn}}}{\rho}}. \tag{A1}$$

TABLE I. Characteristics of the balance.

Forces	X	Y	Z
Capacities (N)	5000±10 000	+5000/ − 10 000	
Accuracy (%)	0.05	0.05	0.1

TABLE II. Characteristics of the balance.

Moments	L	M	N
Capacities (N.m)	$5000 \pm 10\,000$	$+5000/-10\,000$	

2. Boundary layer

At the entrance of the test section, 1 m ahead of the turntable, boundary layer suction is applied through a slot which reduces the boundary layer thickness to 2 cm.

3. Balance

The aerodynamic forces on the cyclist are measured using a six components aerodynamic balance integrated in the rotating turntable just underneath the floor of the test section. The balance is made of three loadcells to measure the vertical load (Z), the pitch moment (M) and the roll moment (L), two horizontal loadcells to measure the sideforce (Y) and the yaw moment (N), and one longitudinal loadcell to measure the drag (X). To attenuate the effects of the mass of the object to be tested and minimize the cross-talking interactions between the vertical and horizontal forces, the vertical loadcells are fitted onto hydraulic conical supports on their nonweighted sides.

The characteristics of the balance are given in Tables I and II:

4. Cyclist setup

The setup used for the cyclist is made of two support plates (front and rear) fitted on the center interfaces of the floor balances [Fig. 12(c)]. These two support plates hold a pair of vertical struts to connect the bike at its wheel axis. The lateral and longitudinal positions of the struts are adjustable. When held by the struts, the wheels sit on the top of two rollers, embedded in the plates. These rollers are motorized by DC motors controlled from the wind tunnel control room. The speed of the wheels is set accordingly to the wind speed. Depending on the bike, the rear wheel can be driven either by its motor or by the cyclist.

---

[1] K. Drais, The Velocipede or Draisena, The Analectic Magazine, pp. 518–519, 1819.

[2] Badwochenblatt, Badwochenblatt für die Großherzogliche Stadt Baden, 24 (1817), https://commons.wikimedia.org/wiki/File:Drais_-_Badwochenblatt_-_Ausschnitt.png.

[3] F. Malizia and B. Blocken, Bicycle aerodynamics: History, state-of-the-art, and future perspectives, J. Wind Eng. Industr. Aerodyn. 200, 104134 (2020).

[4] D. V. Herlihy, *Bicycle: The History* (Yale University Press, New Haven, CT, 2004).

[5] D. G. Wilson and T. Schmidt, *Bicycling Science*, 4th ed. (MIT Press, Cambridge, MA, 2020).

[6] T. N. Crouch, D. Burton, Z. A. LaBry, and K. B. Blair, Riding against the wind: A review of competition cycling aerodynamics, Sports Eng. 20, 81 (2017).

[7] P. E. di Prampero, G. Cortili, P. Mognoni, and F. Saibene, Equation of motion of a cyclist, J. Appl. Physiology 47, 201 (1979).

[8] J. C. Martin, D. L. Milliken, J. E. Cobb, K. L. McFadden, and A. R. Coggan, Validation of a mathematical model for road cycling power, J. Appl. Biomech. 14, 276 (1998).

[9] P. Schepers and K. Klein Wolt, Single-bicycle crash types and characteristics, Cycling Res. Int. 2, 119 (2012).

[10] D. M. Fintelman, M. Sterling, H. Hemida, and F.-X. Li, The effect of crosswinds on cyclists: An experimental study, Proc. Eng. 72, 720 (2014).

[11] D. M. Fintelman, Influence of cycling position and crosswinds on performance and aerodynamics, Ph.D. thesis, School of Sport, Exercise and Rehabilitation Sciences, The University of Birmingham, 2015.

[12] B. Blocken, T. van Druenen, Y. Toparlar, F. Malizia, P. Mannion, T. Andrianne, T. Marchal, G. J. Maas, and J. Diepens, Aerodynamic drag in cycling pelotons: New insights by CFD simulation and wind tunnel testing, J. Wind Eng. Industr. Aerodyn. **179**, 319 (2018).

[13] P. Kraemer, M. Marro, H. Correia, and P. Salizzoni, Preliminary study on crosswind aerodynamics for a group of road race cyclists, SN Appl. Sci. **3**, 279 (2021).

[14] O. Isvan, Wind speed, wind yaw and the aerodynamic drag acting on a bicycle and rider, J. Sci. Cycling **4**, 42 (2015).

[15] R. Garrett, *The Symmetry of Sailing: The Physics of Sailing for Yachtsmen* (Sheridan House, Sheridan, NH, 1996).

[16] L. Brownlie, P. Ostafichuk, E. Tews, H. Muller, E. Briggs, and K. Franks, The wind-averaged aerodynamic drag of competitive time trial cycling helmets, Proc. Eng. **2**, 2419 (2010).

[17] N. Barry, A new method for analysing the effect of environmental wind on real world aerodynamic performance in cycling, Proceedings **2**, 211 (2018).

[18] C. Bourlet, *Traité des bicycles et bicyclettes* (Gauthier-Villars et fils, 1894).

[19] D. M. Fintelman, H. Hemida, Sterling, and F.-X. Li, CFD simulations of the flow around a cyclist subjected to crosswinds, J. Wind Eng. Industr. Aerodyn. **144**, 31 (2015).

[20] S. F. Hoerner, *Fluid-Dynamic Drag* (Hoerner Fluid Dynamics, Brick Township, NJ, 1965).

[21] C. Cohen, E. Brunet, J. Roy, and C. Clanet, Physics of road cycling and the three jerseys problem, J. Fluid Mech. **914**, A38 (2021).